CRYSTAL GROWTH & DESIGN

Article

Cite This: Cryst. Growth Des. 2018, 18, 4611−4620

pubs.acs.org/crystal

Naica's Giant Crystals: Deterioration Scenarios

Iván J. A. Carreño-Marquez,[†] Esperanza Menéndez-Méndez,[‡] Hilda E. Esparza-Ponce,[†] Luis Fuentes-Cobas,[†] Ricardo García-Rovés,[‡] Isaí Castillo-Sandoval,[†] Mayra Luna-Porres,[†] José de-Frutos-Vaquerizo,[§] and María E. Montero-Cabrera*[,†]

[†]Centro de Investigación en Materiales Avanzados (CIMAV), Miguel de Cervantes 120, Complejo Industrial Chihuahua, C.P. 31136 Chihuahua, Mexico

[‡]Instituto Eduardo Torroja de Ciencias de la Construcción, Serrano Galvache 4, 28033, Madrid, Spain

[§]Escuela Técnica Superior de Ingenieros de Telecomunicación, Universidad Politécnica de Madrid, 28040, Madrid, Spain

ABSTRACT: The Cave of Giant Crystals of Naica (Chihuahua, Mexico) is a world geological treasure worth to be preserved. These crystals of up to 12 m in length are made of selenite, the macrocrystalline variety of gypsum ($CaSO_4 \cdot 2H_2O$). They have grown for thousands of years until the cave was dried, which allowed the cave and the crystals to be accessible, but exposed their surfaces in contact with air. Gypsum crystals are fragile because of their trend to dehydrate, the possible replacement to $CaCO_3$ upon reactions with atmospheric CO_2 as well as their intrinsic mechanical properties. Several laboratory experiments, designed to study the deterioration of selenite crystals under different artificial atmospheric conditions, are presented. Four atmospheric compositions rich in CO_2, CH_4, NO_x, and air were tested for 1 year at temperatures of 25 and 60 °C and in either liquid or gaseous environments. The surface evolution was monitored by optical microscopy, infrared spectrometry, and grazing incidence X-ray diffraction with two-dimensional detectors. Surface alteration and dissolution in a water environment were observed in short exposition times, as well as the formation of bassanite ($CaSO_4 \cdot {}^1/_2H_2O$). Neither anhydrite nor calcite was detected. The gaseous environment constituted the most detrimental conditions to the gypsum crystals integrity.

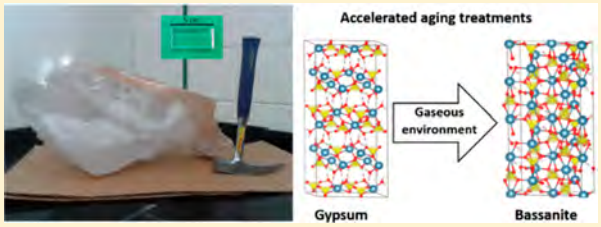

1. INTRODUCTION

1.1. Naica and the Giant Crystals. Naica is a mining town located in the southeastern region of the state of Chihuahua, Mexico (North 27°51′20″ West 105°27′00″) at an altitude of 1330 m above sea level. This area is one of the leading producers of lead, silver, and zinc in the country. Exploitation of the area goes back to the late 18th century, although the first major extraction efforts started in the late 1800s.[1]

The region where the mine is located is formed by three minor mountain chains that constitute an elongated dome in the NW-SE direction, with a series of faults in various orientations.[2] In some cavities related to these faults is where crystals have been able to grow. The cave named "Cueva de las Espadas" (Cave of Swords), located at a level of −120 m below the entrance to the mine, has been known since 1910[3] and contained gypsum crystals up to 2 m long.[4] However, since the first decade of the 21st century, several caves have been discovered around the level −290 m. One of the most outstanding formations is located in "Cueva de los Cristales Gigantes" or Cave of Crystals. In this particular gallery, the crystals span more than 12 m in length.[5] Another recently discovered cave is "Ojo de la Reina" (Queen's eye), which contains smaller crystals,[6] and the "Cueva de las Velas" (Cave of the candles), where the structures are thin and delicate with a few centimeters in size.[7] Figure 1 presents a schematic cross section of the mine, with the location of the two main different caves containing crystals.

The first notable efforts to describe the crystalline phases of Naica's crystals can be traced back to the early 20th century.[8] Nowadays, the mechanisms for the nucleation and growth of large selenite crystals[5] and their growth mechanisms and kinetics[9,10] have been established. In Figure 2, several images of the Cave of Crystals, taken by the authors, are presented.

The giant formations of Naica have been a popular theme in recent years. Although they are not the only giant structures of gypsum known,[11,12] they are the most famous and recognized.[13] Several studies have been executed on Naica's giant gypsum crystals since its discovery.[5,13−15] It has been determined that the crystals begin their nucleation and growth in a slightly supersaturated solution of $CaSO_4$ about half a million years ago[5] with a growth rate of 1.4×10^{-5} nm·s^{-1}.[10]

Currently, the Cave of Crystals is exposed to an air atmosphere with a relative humidity close to 100% and temperatures between 50 and 60 °C.[5] The temperature of this and other caves in Naica are maintained by the action of an intrusion in the area.[16] Additionally, mining extraction commonly releases gases such as CO_x, NO_x, and CH_4 from

Received: April 17, 2018
Revised: June 1, 2018
Published: June 5, 2018

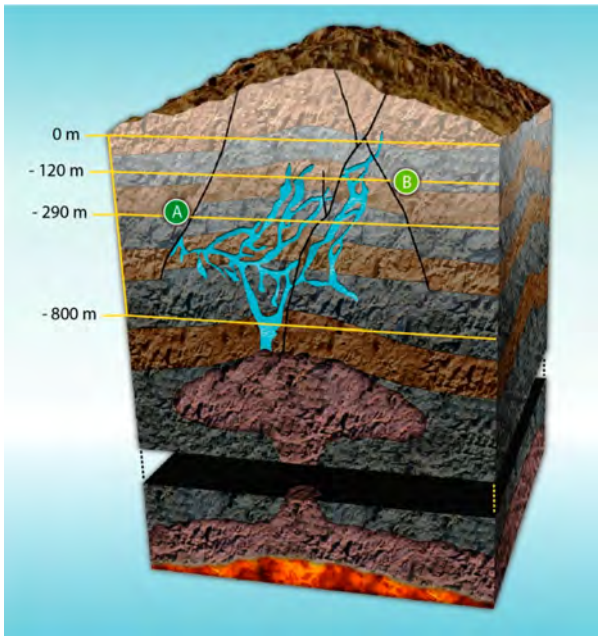

Figure 1. Naica mine cross section. Magmatic intrusion is shown in red; blue lines describe the mineralization. (A) Cave of Crystals and (B) Cave of Swords locations. Adapted with permission from García-Ruiz, J. M.; et al. *Geology* **2007**, *35* (4), 327−330. Copyright 2007 The Geological Society of America.

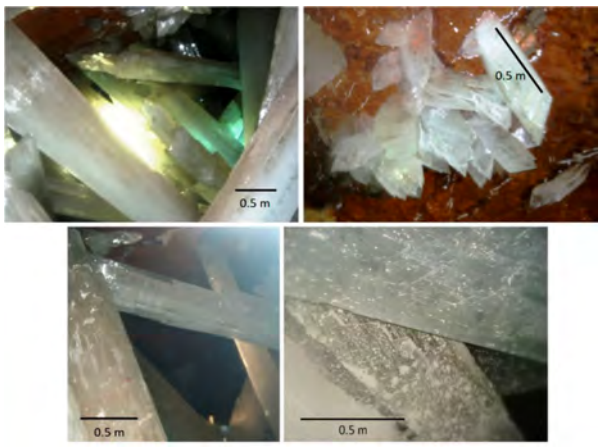

Figure 2. Images of several examples of gypsum crystals found *in situ* in the Cave of Crystals.

underground blasts.[17] Furthermore, CO_2 concentration could increase in semiclosed systems due to breathing.[18,19] Naica mine does not publish air quality studies, but it is assumed that the gases present in the complex are the standard in the mining industry. A lock was installed to separate the crystals cave from their surroundings,[13] generating several possible climatic scenarios depending on if the cave is open or closed.

1.2. Chemical and Crystallographic Information. Calcium sulfate ($CaSO_4$) and its various hydrated forms are widely distributed over the earth's crust. Depending on its state of hydration, three variants of calcium sulfate can be found: anhydrite ($CaSO_4$), hemihydrate or bassanite ($CaSO_4{\cdot}^1/_2H_2O$), and gypsum ($CaSO_4{\cdot}2H_2O$). The crystalline structures of these varieties have important differences, all of them based on a coordination polyhedra formed by sulfate ions. These anions stabilize Ca^{2+} cations that present a coordination number of 8 or 9.[20] The highly transparent samples of macroscopic gypsum crystals are known as selenite, after the Greek goddess of the Moon.

Gypsum is a common evaporite in the world, which is often associated with other minerals such as limestone or shale, in hydrothermal zones or even on Mars.[21,22] Bassanite is a metastable phase[23] and, at the industrial level, is obtained by partial dehydration of gypsum at temperatures from 80 to 180 °C.[24] The structure of the bassanite consists of a molecule of $CaSO_4$ associated with 0.5 molecules of H_2O; although some authors suggest that species such as $CaSO_4{\cdot}0.6H_2O$[25] or even $CaSO_4{\cdot}0.81H_2O$[26] can be found with relative frequency, others argue that the presence of more than 0.5 water molecules tied to calcium sulfate is unlikely to occur.[27] On a gypsum substrate, the bassanite grows heteroepitaxially on the faces (100) and (010), maintaining the direction of the Ca and SO_4 chains.[28]

In Figure 3a, the crystalline gypsum network generates planes of water molecules, in concordance with its primary

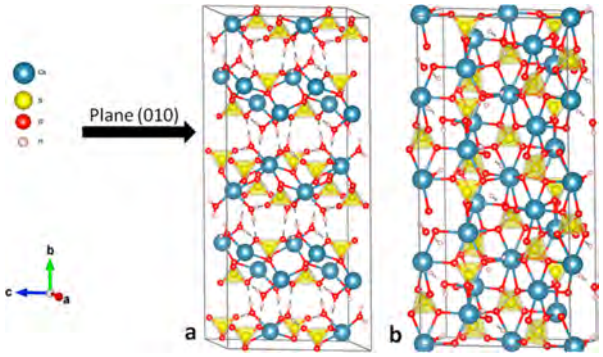

Figure 3. Calcium sulfate structure. (a) In gypsum ($CaSO_4{\cdot}2H_2O$), the water molecules forming the plane (010) are seen. (b) In bassanite ($CaSO_4{\cdot}^1/_2H_2O$), the water molecules reorganize and form channels.

cleavage plane, the (010) plane. In the case of bassanite (Figure 3b), once the dehydration occurs, the remaining water molecules rearrange to form water channels.

For the identification of the different phases of calcium sulfate, both infrared spectrum and X-ray diffraction are widely used. The reported infrared spectra for gypsum and bassanite are similar to each other, with some particular signal differences that make it possible to distinguish between phases.[29] Sulfate ion presents its characteristic bands in ranges smaller than 1200 cm^{-1}.[30] The v3 vibrations in the bassanite differ slightly from the other calcium sulfates: like the one at 1180 cm^{-1}, which is not present in gypsum.[31]

In relation to X-ray diffraction patterns, the Kα radiation of a Cu source (1.5418 Å wavelength) produces the main reflection of gypsum from the plane (020) at $2\theta \approx 11.6°$, while the main signal of bassanite arises at 14.8° for the plane (110). Due to the potential structural differences between the various crystals present in the samples, there may be some small shifts that need to be considered for their identification.[28] Prieto-Taboada et al. have identified bassanite and various types of anhydrite applying standard X-ray diffraction techniques for

DOI: 10.1021/acs.cgd.8b00583
Cryst. Growth Des. 2018, 18, 4611−4620

the analysis of various gypsum samples from both industrial suppliers and natural gypsum samples, like "arrowhead" and "desert rose" formations.[32]

The preservation of the Naica's gypsum crystals is uncertain due to the microclimatic changes introduced by human activity. In a previous laboratory study, the effect of microclimatic conditions, similar to those in the Cave of Crystals, has been tested with the use of accelerated weathering techniques on gypsum single crystals. An atmosphere with high concentrations of CO_2 dissolved in water mist has been tested at temperatures of 51 °C. These conditions lead to a weight loss of about 4%, which indicates that, in conditions comparable to the ones in the Cave of Crystals, the primary concern would be the dissolution of the structures.[33]

The purpose of this work is to experimentally simulate different scenarios to which the crystals could be exposed and to estimate the deterioration that may be generated. To the best of our knowledge, no reports are predicting the future of Naica gypsum giant crystals under microclimatic conditions similar to those tested in the present work. Although the variables which affect the crystals are copious and diverse, gypsum single crystals samples were exposed to four different atmospheres: air, CO_2, CH_4, and NO_x. The same test was also performed under two different conditions: in a gaseous environment and submerged in distilled water, and at different temperatures. Samples were extracted from the reactor at 1, 3, 6, and 12 months, and then characterized by optical microscopy, infrared spectroscopy (IR), and X-ray diffraction (GI-XRD).

2. EXPERIMENTAL METHODS

2.1. Sample Preparation. A selenite bulk 40 kg specimen from the Giant Crystals Cave was obtained through a donation by a private collector. The material provided was characterized by X-ray diffraction to confirm the sample crystal phase as gypsum ($CaSO_4 \cdot 2H_2O$).

Clean samples, as seen in Figure 4, were cut from the volume of the bulk specimen, into fragments of approximately 5 × 3 cm^2, avoiding impurities inclusions. Before the experiments, a thin layer, parallel to its cleavage plane, was assured. On one edge, a small clean cut was made with a scalpel along the cleavage plane; this allowed the detachment of a layer of material and ensured a clean and homogeneous surface.

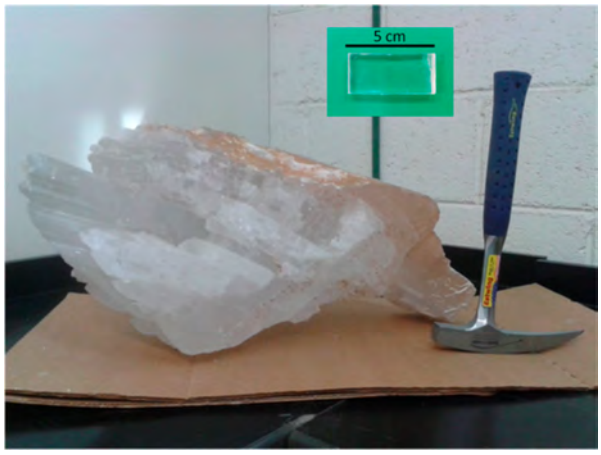

Figure 4. Bulk specimen from Giant Crystals Cave. In the green box, a sample as used in the experimentation can be seen.

2.2. Climate Simulation. To perform an accelerated microclimatic simulation,[34] several reactors were saturated according to most frequent gas releases in mines, described in section 1.1. For each particular atmosphere, two reactors were arranged, one at 25 °C and the other at 60 °C. The temperature of 60 °C was selected because it is high enough to accelerate the probable dehydration process. Nevertheless, it is below the transition temperature of the gypsum to bassanite, which is not going to be produced in the conditions generated by the intrusion in the cave area. All experiments were performed at laboratory pressure, which oscillated naturally between 91 and 96 kPa. Some studies have tested the effect of relative humidity on calcium sulfate and have determined that, at 80%, there is a critical point for the integrity of the material.[35] For this reason, in this work, a relative humidity of 85% was generated within the reactor. As we said before, the samples were extracted at 1, 3, 6, and 12 months. Figure 5 shows (a) a schematic configuration for each reactor, with their respective atmosphere, and (b) the general design of the experimentation. Each extracted sample was not replaced into the reactor.

Regarding the environment of the sample, two configurations were mounted, one where the crystals were in direct contact with the gas, and another where the samples were submerged in a beaker with distilled water, in which the respective gas was bubbled until saturation. This water solution was used to promote accelerated deterioration of the samples. The gas concentration in the liquid environment matches the saturation value predicted by Henry's Law for each temperature. A 22% mass solution of sulfuric acid was placed on the bottom of the reactor, to ensure the relative humidity of 85% in the reactor according to ASTM E-104. Eight reactors were assembled in which a total of 64 samples were placed, corresponding to the same number of microclimatic conditions.

2.3. Optical Appearance. The optical appearance was evaluated in order to measure the effect of the different environments and to observe the formation of superficial alterations.

This indicator was constructed by visual inspection when comparing the sample with an untreated reference crystal. Subsequently, the surface of interest was observed with an Olympus BX51 optical microscope with 4×, 10×, and 20× magnifications. Finally, a stereomicroscopy study, using a cross section of the sample, was performed with a Volpi Intralux 4000 microscope to examine surface damages.

2.4. Infrared Spectrometry. To detect the formation of bassanite or anhydrite as a result of gypsum dehydration, or the formation of calcium carbonate by reaction with atmospheric CO_2, infrared (IR) measurements were performed. A PerkinElmer Spectrum 400 equipment was used in the range of 450−4000 cm^{-1}. The crystals were exposed to the infrared beam with no further treatment on the surface of interest.

2.5. Grazing Incidence X-ray Diffraction. Laboratory and synchrotron GI-XRD were employed for detecting the possible formation of phases other than gypsum.

Laboratory measurements were performed with a Panalytical X'Pert Pro diffractometer with a Cu source. The detector used was a PIXcel^{3D} in two-dimensional (2D) configuration. The samples were analyzed, without any additional preparation, with an incidence angle ϕ of 0.1° and 2θ scans from 10° to 80° in 0.026° steps. The irradiated area was approximately 5 × 5 mm^2.

Synchrotron GI-XRD was carried out at the beamline 11-3 of the Stanford Synchrotron Radiation Lightsource. 2D diffraction patterns were collected on a MAR2300 position-sensitive detector. Measurement parameters were calibrated by use of a LaB_6 standard. The sample−detector distance and the X-ray wavelength were, respectively, 205 mm and 0.9744 Å. Incidence angles scanned from 0.05° to 0.15°. The measurements on the area of interest were made through a 5 × 5 points mesh, with steps of 0.5 mm in both directions. Beam size was of 50 μm vertical × 150 μm horizontal. Debye rings data in 2D patterns were integrated by use of the WXDIFF and ANAELU programs.[36,37] Integrated 1D patterns were matched with those of gypsum and considered additional phases.[38]

DOI: 10.1021/acs.cgd.8b00583
Cryst. Growth Des. 2018, 18, 4611−4620

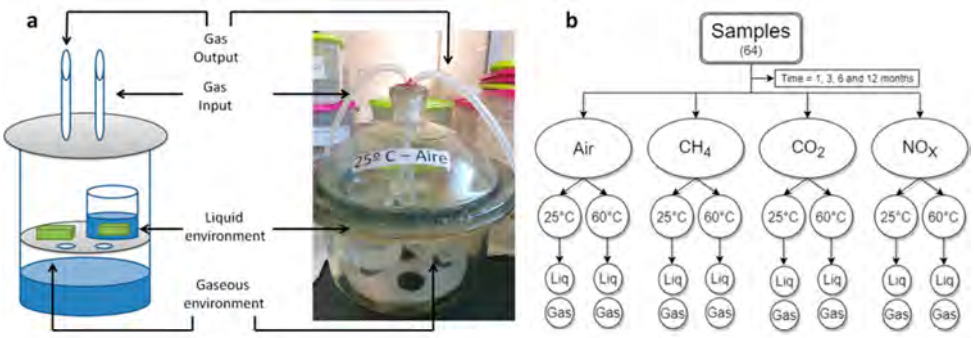

Figure 5. (a) Reactor configuration and (b) general planning of the microclimatic simulation.

2.6. Relative Amount of Bassanite. The present section explains the procedure that has been applied to assign a semi-quantitative descriptor to the relative bassanite occurrence in altered samples. Standard diffraction analysis is performed by measuring the intensities of representative peaks and applying different algorithms, related to the proportionality expressed in the expression (1).

$$\frac{I_\gamma}{I_\alpha} \propto \frac{C_\gamma}{C_\alpha} \quad (1)$$

I_γ and I_α are the summed intensities of the diffraction peaks of bassanite and gypsum, respectively. Each C represents the relative concentration of the corresponding phase. In our experiments, due to samples' rugosity, bassanite geometrical dispersion, and disordered distribution of crystallites orientations, the observed numbers of gypsum and bassanite diffraction peaks and the corresponding diffracted intensities (I_γ, I_α) are weakly correlated. The results of the application of expression (1) in the experiments are denoted in the text as the relative intensity of bassanite.

A semiquantitative descriptor of the relative amount of bassanite (RAB) has been introduced by integrating: (a) the detection of the 1180 cm^{-1} signal in the infrared spectra, (b) the number of bassanite peaks in the integrated GI-XRD (lab and synchrotron) patterns, and (c) the relative intensity of bassanite according to expression (1). Each indicator was normalized to one, dividing by the highest value observed in the whole experimental simulation. The sum of the three mentioned indicators (possible maximum = 3) characterized the relative occurrence of bassanite in a given sample and was used as an index of the deterioration of the gypsum samples.

3. RESULTS

3.1. Optical Appearance. The removal of samples was carefully done with tweezers by the edges of the crystals to prevent affectation of the potentially damaged surface. Samples were kept in a sealed plastic box to prevent contamination. Only five samples presented a remarkable deterioration once they were removed from their respective reactor.

When performing a visual inspection, it could be noticed that some crystals became opaque at some areas of the surface. Figure 6a shows the reference sample for comparison with some selected treated samples. The differences between samples are referred to as alterations. The reference sample presents alterations only at the edges, in which the cleavage planes (010) have been opened by mechanical action. The edges of the sample are therefore more susceptible to modification in the tests, as they present more exposed surface microscopically. Most of the samples showed similar behavior. In Figure 6b–f, the evident opacity and the formation of multiple smaller alterations can be found. Other types of alterations may include the formation of small pits, formation of different kinds of roughness, or small fractures of the surface.

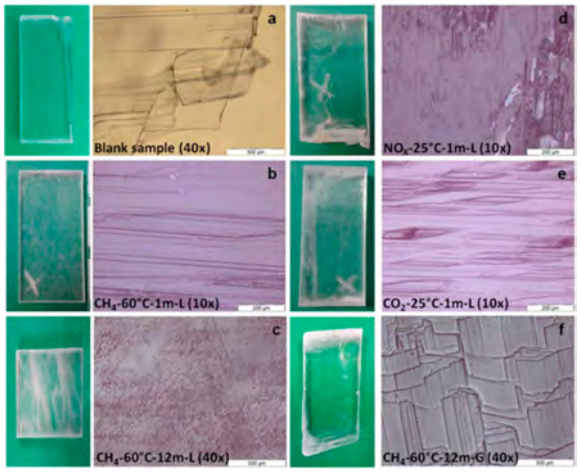

Figure 6. Remarkable damage caused by applied atmospheres. On the left appears a photograph of the sample and, on the right, an optical microscopy image. (a) Gypsum sample without treatment with an optical magnification of 40×. (b) CH_4-60°C-1m-L with 10× magnification. (c) CH_4-60°C-12m-L with 40× magnification. (d) NO_x-25°C-1m-L with 10× magnification. (e) CO_2-25°C-1m-L with 10× magnification. (f) CH_4-60°C-12m-G with 40× magnification. Nomenclature indicates Atmosphere-Temperature-Time-Environment.

In Figure 7a–e, the changes at the surface of the crystals, after being subjected to the climatic simulation, are observed

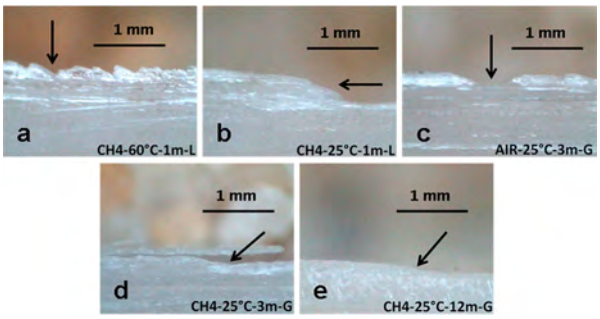

Figure 7. Types of surface damage detected by stereomicroscopy. (a) Irregular. CH_4 at 60 °C for 1 month in liquid. (b) Slope. CH_4 at 25 °C for 1 month in liquid (c) Well. Air at 25 °C for 3 months in gas. (d) Detachment. CH_4 at 25 °C for 3 months in gas. (e) Minor slope. CH_4 at 25 °C for 12 months in gas.

DOI: 10.1021/acs.cgd.8b00583
Cryst. Growth Des. 2018, 18, 4611–4620

on cross section by stereomicroscopy. In Figure 7a–c,e, it can be detected that the cleavage plane, characteristic of the gypsum crystals, generated different types of irregularities. Even in Figure 7d, it can be seen that a small surface layer is detached. Other irregularities can appear in Figure 7c,d. Additionally, during dehydration processes, the atomic rearrangement produced by the loss of 1.5 water molecules generates mechanical stress in the structure, as seen in Figure 3b. The presence of irregularities and the appearance of other phases may cause the alteration of mechanical properties, which may produce detachments in layers close to the surface of the crystal.[39]

The overall surface alteration of the samples was assessed, giving values to three features: visual evaluation, optical microscopy, and stereomicroscopy. To those samples which did not show a given deterioration, a value of 0 was assigned, while moderate damage was valued with 0.5 and severe damage with 1. The three values were summed, and the resulting assessment can be found in Table 1.

Table 1. Surface Alteration Data[a]

Atmosphere	Time	Environment: Liquid 25°C a	b	c	SA	Liquid 60°C a	b	c	SA	Gas 25°C a	b	c	SA	Gas 60°C a	b	c	SA
Air	1m	0	0	1	1	0	0	0	0	0.5	0	0.5	1	0.5	0.5	0.5	1.5
	3m	0	0	1	1	0	0	0	0	1	0	0.5	1.5	0	0.5	0	0.5
	6m	0	0	0	0	0	0	0	0	0	0	0	0	0	0	1	1
	12m	0.5	0.5	0	1	0	0.5	0	0.5	0.5	0.5	0	1	1	0	0	1
CH_4	1m	0	0	0.5	0.5	1	0.5	1	2.5	0	0.5	0.5	2	0	0	0.5	0.5
	3m	0	0	0.5	0.5	0	0.5	0.5	1	0	0	0.5	0.5	0	0.5	0	0.5
	6m	0	0	0	0	0	0	0	0	0	0	0	0	0	0	0	0
	12m	0.5	0	0	0.5	1	1	0	2	0.5	0	0	0.5	0	1	0	1
CO_2	1m	0.5	0.5	1	2	0	0	0	0	0.5	0.5	1	2	0.5	0	1	1.5
	3m	0	0.5	0.5	1	0	0.5	0	0.5	0	0	0	0	0	0.5	0.5	1
	6m	0	0	0	0	0	0	0.5	0.5	0	0	0	0	0	0	0	0
	12m	0.5	0	0	0.5	0.5	0	0	0.5	0	0	0	0	0	0	0	0
NOx	1m	0.5	0	0.5	1	0.5	0.5	0.5	1.5	0	0.5	0.5	1	0.5	0.5	0.5	1.5
	3m	0	0	0	0	0	0	0.5	0.5	0	0	0.5	0.5	0	0	0	0
	6m	0	0	0	0	0.5	0.5	0	1	0	0	0	0	0.5	0	0	0.5
	12m	0.5	0	0	0.5	0.5	0	0	0.5	0	0	0	0	0	0	0	0

[a]a, optical appearance; b, optical microscopy; c, stereomicroscopy; SA, surface alteration = a + b + c.

Analyzing the results of this section, several samples showed irregularities in their surface as a consequence of the treatment applied to them. This behavior has already been observed in some specimens of Cave of Crystals.[40] The damage caused in similar systems has been reported in the past decades. Sipple et al. report the fracture of the surface in gypsum single crystals parallel to the cleavage plane (010), but do not describe the factors that cause it.[41] However, the dehydration process of a sample affects the incidence of cracks in the plane (010), which may be oriented in different crystallographic planes.[42] Gypsum presents deformations when shear stress on the plane (010) is applied, creating displacements and fractures of mechanical origin;[43] these deformations can be more severe at a higher temperature.[44] The observed behaviors of the samples in our microclimatic simulations agree with those reported phenomena.

Likewise, the dissolution of the samples and the relative humidity to which they are exposed play a decisive role in the formation of irregularities on the crystal surface.[45,46] These authors have observed and reported the dissolutions of gypsum single crystals, similar to those used in this work, as a loss in the weight of the samples.[33] These phenomena, measured in the laboratory, have also been verified *in situ* in mining systems with native gypsum.[38] Other studies, such as the one conducted in "Cueva del Agua" in Granada, Spain, warn that, even under normal conditions, water condensation on native speleothems may constitute a risk of corrosion.[47]

3.2. Infrared Spectrometry. Typical IR spectra for gypsum were found in all cases. Additionally, signals with values of about 1180 cm^{-1} were obtained in several samples, which were considered as samples containing bassanite. The possible signals for calcium carbonate were about the detection limits of the experiments. In Figure 8, selected spectra can be observed: in orange, a signal at 1180 cm^{-1} can be detected for the sample CO_2-60°C-3m-L; in red, the sample CH_4-60°C-3m-G where the signal may be under the detection limits; and in blue, a blank gypsum sample without this signal. Signals between 1600 and 1700 cm^{-1} are related to bending modes $\nu 2$ of water. Near 1620 cm^{-1}, both bassanite and gypsum peaks can appear. An increase in the signal intensity can be attributed to the appearance of bassanite.[31]

In Table 2, the samples that produced the vibration v3 as an indicator of bassanite manifestation are shown.

All the 64 samples were analyzed, and 22 presented the 1180 cm^{-1} "bassanite" signal. From these 22 samples, 15 underwent exposition times of 6 and 12 months to different microclimates, most of them being surrounded only by gas. These

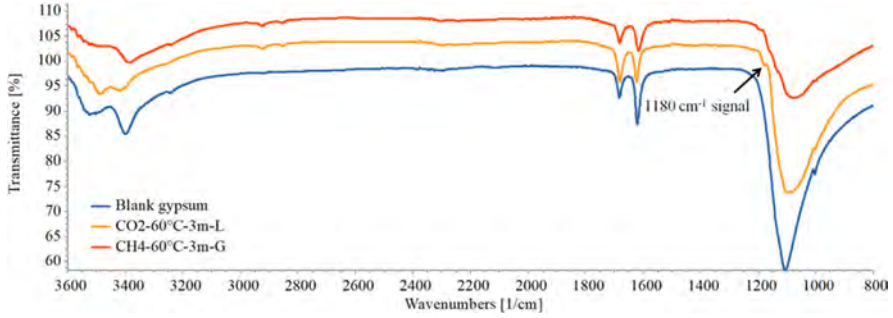

Figure 8. IR spectra for selected samples: (blue) blank gypsum sample; (orange) sample with the characteristic 1180 cm^{-1} signal; and (red) sample with a signal below the detection limit. Bassanite was identified in combination with gypsum signals.

DOI: 10.1021/acs.cgd.8b00583
Cryst. Growth Des. 2018, 18, 4611–4620

Table 2. Assessment of the 1180 cm^{-1} Vibration v3 as an Indicator of Bassanite Presence[a]

Atmosphere	Time (months)	Environment: Liquid 25°C	Liquid 60°C	Gas 25°C	Gas 60°C
Air	1	-	-	+	-
	3	-	-	-	-
	6	+	+	+	-
	12	-	-	-	-
CH_4	1	-	-	-	-
	3	-	-	+	-
	6	-	-	+	+
	12	+	-	-	+
CO_2	1	-	-	-	-
	3	-	-	-	+
	6	-	-	-	+
	12	-	-	+	-
NOx	1	+	-	+	-
	3	+	-	+	-
	6	+	+	-	+
	12	-	+	+	+

[a]Symbol + means detection of the vibration.

results suggest a higher production of bassanite in long exposure times, in gaseous environments.

These features are in accordance with calcium sulfate infrared patterns studied in depth by several authors. Sarma et al. studied the phase transitions of calcium sulfate in natural gypsum samples from India. Analyzing these vibrations, they were able to observe the dehydration process in gypsum until its ultimate transformation into anhydrite.[48] Additionally, Lane successfully studied the IR emission spectrum of different sulfate minerals, identifying the role of water molecules in the sulfate vibrations, as well as the vibration near 1180 cm^{-1}.[49]

3.3. Semiquantitative Analysis by Grazing Incidence X-rays Diffraction. GI-XRD experiments were performed on all the samples. Samples tested during 1 month were not assigned a deterioration index because none of them had bassanite diffraction peaks above the detection limits. In all the other GI-XRD diffraction patterns, distinctive bassanite reflections were detected in changing numbers and with variable intensities, indicating differences of their bassanite relative concentration. On the other hand, calcium carbonate peaks with statistically significant intensities were not detected in any sample.

Figure 9 shows two selected laboratory diffractograms that illustrate different sample behaviors. The sample (red) exposed to NO_x at 25 °C for 6 months in liquid shows only gypsum reflections, especially the main plane (010), while the sample (blue) exposed to NO_x at 60 °C for 6 months in gas shows several bassanite reflections and a wide variety of gypsum peaks. The relative intensities of the gypsum and bassanite peaks do not follow regular patterns due to the existing irregularities on the samples surfaces.

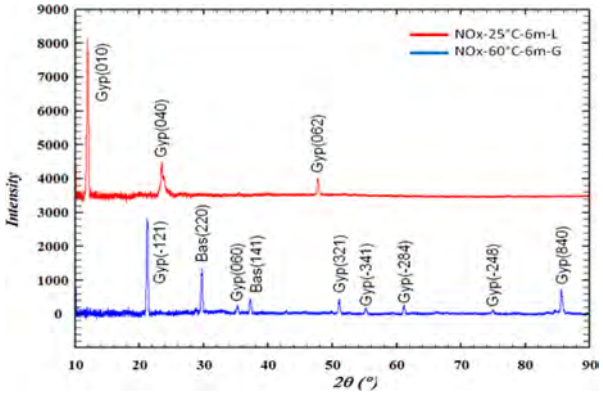

Figure 9. GI-XRD patterns integrated from a two-dimensional measurement of one sample with no bassanite signals (red), and another sample with gypsum (Gyp) and bassanite (Bas).

Figure 10 represents, as a representative case, the 1D XRD patterns of the CH_4 atmosphere at 25 °C in a gaseous

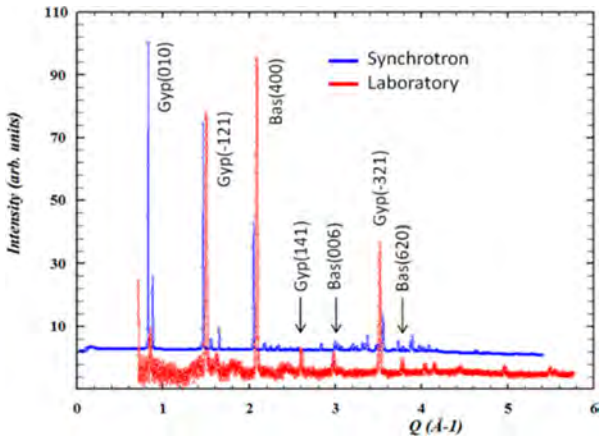

Figure 10. Comparison of laboratory and synchrotron XRD patterns of a bassanite-containing sample. Gypsum and bassanite peaks are identified for the CH_4-25°C-3m-G sample.

environment treated for 3 months, obtained from 2D spectra measured with laboratory (red) and synchrotron (blue) devices. A synchrotron signal was obtained by the integration of the mesh of 25 different zones in the same sample, while the laboratory pattern was obtained by the integration of the linear pattern produced by the PixCEL[3D] detector. Patterns have been plotted in the $Q\left(=\frac{4\pi}{\lambda}\sin\vartheta\right)$ domain (independent of wavelength), normalized to I_{max} = 100 and shifted vertically to facilitate visualization. The difference between counting statistics is apparent. The small random shifts in the Q positions of diffraction maxima are a consequence of the grazing incidence experimental configuration.[50] Synchrotron diffraction confirms the laboratory detection of bassanite.

Table 3 shows the evaluation of bassanite relative intensities, obtained by expression (1), expressed in percent (%) for samples tested.

3.4. Overall Results. The results of all observations were statistically evaluated using Minitab 16 software. The analyzed quantities were: the overall optical appearance, the v3 vibration feature from IR spectra, and the relative intensity of bassanite

DOI: 10.1021/acs.cgd.8b00583
Cryst. Growth Des. 2018, 18, 4611−4620

Table 3. Relative Intensity of Bassanite (%), Determined by GI-XRD[a,b]

		Liquid environment			Gaseous environment		
Atmosphere	Temperature (°C)	3 Months	6 Months	12 Months	3 Months	6 Months	12 Months
AIR	25	DL	5	37	23	57	42
	60	37	24	15	9	44	1
CO_2	25	28	15	18	14	22	18
	60	14	63	11	43	50	9
CH_4	25	6	16	56	46	63	44
	60	42	24	12	34	9	17
NOx	25	18	DL	64	7	27	56
	60	5	8	72	60	21	15

[a]The higher values for each atmosphere are highlighted. [b]DL = Below detection limits.

Table 4. Relative Amount of Bassanite (RAB)

		Liquid environment			Gaseous environment		
Atmosphere	Temperature (°C)	3 Months	6 Months	12 Months	3 Months	6 Months	12 Months
AIR	25	0.78	0.89	1.10	1.43	2.40	1.70
	60	1.32	1.54	1.09	1.20	1.58	1.95
CO_2	25	0.67	1.39	1.08	1.24	1.03	0.84
	60	1.00	1.33	1.34	1.55	1.78	1.39
CH_4	25	0.21	1.05	1.65	2.09	2.81	1.41
	60	0.99	0.48	0.90	1.22	0.89	0.48
NOx	25	0.92	0.83	1.00	1.51	1.19	1.37
	60	0.41	0.55	0.66	1.58	1.49	1.29

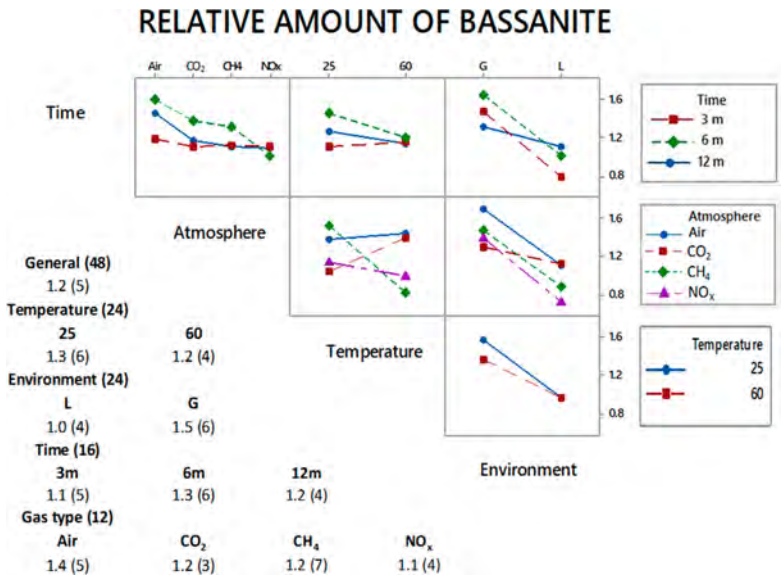

Figure 11. Trends in the relative amount of bassanite. The values in the table are presented in "ε (σ)" format.

from GI-XRD results. A multivariate analysis of variance (MANOVA) of the measured quantities was performed, with $p < 0.05$ to find statistically significant differences between the results. The factors for statistical analysis were the following microclimatic variables: atmosphere (with four different gases), temperature (2 values), environment (2 phases), and exposure time (4 values). In cases where significant differences were found within the MANOVA test, Tukey's post-hoc test was

DOI: 10.1021/acs.cgd.8b00583
Cryst. Growth Des. 2018, 18, 4611−4620

performed to identify which of the factors made the statistical differences. The applied statistical tests corroborated that the results of bassanite detection by both IR and GI-XRD in the gaseous environment are significantly different from those of the liquid environment.

The RAB results are presented in Table 4 and were analyzed by the following two methods. (a) In the graphic of Figure 11 are presented the RAB results, taking each value of the four different atmospheres, the two temperatures, the three exposure times, or the two environments as a parameter. Once a parameter as constant was selected, the results corresponding to the other variables were averaged. In total, the graphic presents the tendencies for the six possible combinations of independent parameters. (b) The table of Figure 11 presents the averages ε and the standard deviations σ of the statistical sampling of the RAB presented in Table 4, over 24 different values for each temperature, 24 for each environment, 12 for each atmosphere, and 16 for each exposure time.

From Figure 11, it may be observed that the relative amount of bassanite does not show a definite trend as a function of atmosphere and temperature, or time and temperature. The time−atmosphere relation suggests that the highest proportion of bassanite is produced in air, followed by CO_2. The time−environment, atmosphere−environment, and temperature−environment relations suggest that the gaseous environment provides a higher amount of bassanite than the liquid one.

The RAB is relevant for the determination of crystal damage. The generation of contaminating phases harms the cultural treasure condition of the crystals. Eventually, the dehydration of the substrate would destroy the crystals.

4. DISCUSSION

Several studies have shown that temperature is a crucial factor in the transition from gypsum to bassanite and later to anhydrite.[51] Nevertheless, the concept of transition temperature in phase equilibrium does not prohibit the appearance of phases at temperatures lower than equilibrium.[52] On Mawrth Valley, located on Mars, bassanite deposits have been found despite the extreme thermal and aqueous conditions.[53] This contradicts previous statements regarding bassanite formation. The decrement in water activity can be linked to bassanite stability in low water activity environments,[54] while other studies have found a plausible pathway to bassanite formation at room temperature.[55]

Human activities suppose the production of carbon dioxide for both, natural and artificial means. It has been found that CO_2 can dramatically increase its natural concentration in semiclosed systems by the effect of the presence of people and thus affect the crystals.[18,19] Badino et al. found calcium carbonate ($CaCO_3$) precipitation in some gypsum structures in Candles Cave, a nearby cave in the Naica system.[6] However, in the present microclimatic simulations, no carbonates were detected, even in the presence of a CO_2 atmosphere as a possibility suggested by other studies.[56] In addition to this, the extraction of minerals in Naica involves the combustion of different energy sources; therefore, the presence of other gases such as NO_x and CH_4 is reasonable. The action of these gases, in combination with the relative temperatures and humidity of the site, could induce the formation of acids that compromise the integrity of the crystals,[57] although they have not been observed in the present experiment. Most of the samples presented a dehydration process which triggered the formation of bassanite ($CaSO_4 \cdot {}^1/_2H_2O$). The presence of anhydrite on the surface of the crystals was not experimentally detected in the present work. By the conditions under which the anhydrite is generated and the ease with which it is hydrated from the ambient humidity, it is highly unlikely that it has been produced during the tests.

5. CONCLUSIONS

Diverse microclimatic scenarios were experimentally simulated, revealing that the most detrimental condition to the crystals is a gaseous environment. Air atmosphere proved to be the most dangerous to the crystals integrity. These conditions can trigger a chain of events that may include corrosion, dissolution, mechanical breakage, and surface alterations. The most relevant transformation is produced by the dehydration of gypsum into bassanite, which has different physical properties than gypsum.

It is important to remark that the current conditions in the Cave of Crystals are similar to those found to be the most detrimental. This suggests that surface transformations may be happening right now on the giant crystals. Therefore, the best possible scenario is the restoration of its original conditions or the adequate protection against potentially dangerous environments caused by the presence of an altered atmosphere. This protection would include the creation of an independent entrance to the Cave of Crystals or the creation of an *ex situ* exhibition that limits the interaction of the crystals with potentially aggressive circumstances.

Several studies and conservation efforts, in caves with particular geologic or touristic relevance, have been made around the world. In them, close coordination among academia, private sector, and government has allowed generating a series of public policies that permit preserving these geological treasures. This work aims at contributing to an empirical knowledge that would lead to the preservation of the Naica's Giant Gypsum Crystals. For this reason, and for the first time, different plausible microclimatic conditions were tested on gypsum crystals demonstrating which are the most detrimental.

AUTHOR INFORMATION

Corresponding Author

*Phone: +52 614 439 1100, ext. 1123. E-mail: elena.montero@cimav.edu.mx.

ORCID

María E. Montero-Cabrera: 0000-0002-1906-0105

Notes

The authors declare no competing financial interest.

ACKNOWLEDGMENTS

The authors would like to acknowledge Consejo Nacional de Ciencia y Tecnologia (grant number 183706); Industrias Peñoles for the support given to the experiments; A. Reyes-Rojas, D. Burciaga-Valencia, and E. Guerrero-Lastarjette for their continuous support in the realization of this project; and B. Aldea-Ballano and the team of the Chemical and Physicochemical Testing Unit in Instituto Eduardo Torroja de Ciencias de la Construcción in Madrid. The authors especially thank J. M. García-Ruiz for the suggestions of some experiments. Part of the experiments was performed (as part of Proposal No. 3939) at the Stanford Synchrotron Radiation Lightsource (SSRL), a Directorate of SLAC National

DOI: 10.1021/acs.cgd.8b00583
Cryst. Growth Des. 2018, 18, 4611−4620

Accelerator Laboratory and an Office of Science User Facility operated for the U.S. Department of Energy, Office of Science, by Stanford University. The authors would like to acknowledge the discussions and suggestions of the anonymous reviewers.

REFERENCES

(1) Stone, J. G. Ore genesis in the Naica district, Chihuahua, Mexico. *Econ. Geol. Bull. Soc. Econ. Geol.* **1959**, *54* (6), 1002−1034.
(2) Marín-Herrera, B. R.; Vogel Gonzalez, F.; Echegoyen Guzman, R. Las megaselenitas del distrito minero de Naica, Chihuahua, una ocurrencia mineralogica anomala. *Bol. Mineral.* **2006**, *17*, 139−148.
(3) Wittich, E.; Pastor-Giraud, A. Unos cristales gigantes de yeso procedentes de la mina Naica, Chihuahua. *Bol. Soc. Geol. Mex.* **1912**, *8*, 61−70.
(4) Foshag, W. The gypsum caves of Naica, Mexico. *Am. Mineral.* **1927**, *12* (6), 252−256.
(5) Garcia-Ruiz, J. M.; Villasuso, R.; Ayora, C.; Canals, A.; Otalora, F. The Formation of Gypsum Megacrystals. *Geology* **2007**, *35* (4), 327−330.
(6) Badino, G.; Calaforra, J. M.; Forti, P.; Garofalo, P.; Sanna, L. The present day genesis and evolution of cave minerals inside the Ojo de la Reina Cave (Naica Mine, Mexico). *Int. J. Speleol.* **2011**, *40* (2), 125−131.
(7) Bernabei, T.; Forti, P.; Villasuso, R. Sails: a new gypsum speleothem from Naica, Chihuahua, Mexico. *Int. J. Speleol.* **2007**, *36*, 23−30.
(8) Posnjak, E. The system $CaSO_4$-H_2O. *Am. J. Sci.* **1938**, *235A*, 247−272.
(9) van Driessche, A. E. S.; García-Ruiz, J. M.; Delgado-Lopez, J. M.; Sazaki, G. In Situ Observation of Step Dynamics on Gypsum Crystals. *Cryst. Growth Des.* **2010**, *10* (9), 3909−3916.
(10) van Driessche, A. E. S.; García-Ruíz, J. M.; Tsukamoto, K.; Patiño-Lopez, L. D.; Satoh, H. Ultraslow growth rates of giant gypsum crystals. *Proc. Natl. Acad. Sci. U. S. A.* **2011**, *108* (38), 15721−15726.
(11) Bozeman, J.; Bozeman, S. Speleology of gypsum caves in Oklahoma. *Carbonates Evaporites* **2002**, *17* (2), 107−113.
(12) Boidin, E.; Homand, F.; Thomas, F.; Yvon, J. Anhydrite−gypsum transition in the argillites of flooded salt workings in eastern France. *Environ. Geol.* **2009**, *58* (3), 531−542.
(13) Gázquez, F.; Calaforra, J. M.; Forti, P.; Badino, G. The Caves of Naica: A decade of research. *Bol. Geol. Min.* **2016**, *127* (1), 147−163.
(14) Forti, P.; Sanna, L. The Naica Project: A multidisciplinary study of the largest gypsum crystals of the world 3. *Episodes* **2010**, *33* (1), 23−32.
(15) Otalora, F.; Garcia-Ruiz, J. Nucleation and growth of the Naica giant gypsum crystals. *Chem. Soc. Rev.* **2014**, *43* (7), 2013−2026.
(16) Alva-Valdivia, L. M.; Goguitchaichvili, A.; Urrutia-Fucugauchi, J. Petromagnetic properties in the Naica mining district, Chihuahua, Mexico: Searching for source of mineralization. *Earth, Planets and Space* **2003**, *55* (1), 19−32.
(17) De Souza, E. M.; Katsabanis, P. D. On the prediction of blasting toxic fumes and dilution ventilation. *Min. Sci. Technol.* **1991**, *13* (2), 223−235.
(18) Baker, A.; Genty, D. Environmental pressures on conserving cave speleothems: Effects of changing surface land use and increased cave tourism. *J. Environ. Manage.* **1998**, *53* (2), 165−175.
(19) Dragovich, D.; Grose, J. Impact of tourists on carbon dioxide levels at Jenolan Caves, Australia: an examination of microclimatic constraints on tourist cave management. *Geoforum* **1990**, *21* (1), 111−120.
(20) Singh, N. B.; Middendorf, B. Calcium sulfate hemihydrate hydration leading to gypsum crystallization. *Prog. Cryst. Growth Charact. Mater.* **2007**, *53* (1), 57−77.
(21) Bishop, J. L.; Lane, M. D.; Dyar, M. D.; King, S. J.; Brown, A. J.; Swayze, G. A. Spectral properties of Ca-sulfates: Gypsum, bassanite, and anhydrite. *Am. Mineral.* **2014**, *99* (10), 2105−2115.
(22) Wray, J. J.; Squyres, S. W.; Roach, L. H.; Bishop, J. L.; Mustard, J. F.; Noe Dobrea, E. Z. Identification of the Ca-sulfate bassanite in Mawrth Vallis, Mars. *Icarus* **2010**, *209* (2), 416−421.
(23) van Driessche, A. E. S., Kellermeier, M., Benning, L. G., Gebauer, D., Eds. *New Perspectives on Mineral Nucleation and Growth: From Solution Precursors to Solid Materials*; Springer International Publishing: Cham, Switzerland, 2017.
(24) Cave, S. R.; Holdich, R. G. The Dehydration Kinetics of Gypsum in a Fluidized Bed Reactor. *Chem. Eng. Res. Des.* **2000**, *78* (7), 971−978.
(25) Bezou, C.; Nonat, A.; Mutin, J.-C.; Christensen, A. N.; Lehmann, M. S. Investigation of the Crystal Structure of γ-CaSO4, $CaSO_4 \cdot 0.5\ H_2O$, and $CaSO_4 \cdot 0.6\ H_2O$ by Powder Diffraction Methods. *J. Solid State Chem.* **1995**, *117* (1), 165−176.
(26) Abriel, W. Calcium sulfat subhydrat, $CaSO_4\ 8H_2O$. *Acta Crystallogr., Sect. C: Cryst. Struct. Commun.* **1983**, *39* (8), 956−958.
(27) Weiss, H.; Bräu, M. F. How Much Water Does Calcined Gypsum Contain? *Angew. Chem., Int. Ed.* **2009**, *48* (19), 3520−3524.
(28) Follner, S.; Wolter, A.; Preusser, A.; Indris, S.; Silber, C.; Follner, H. The Setting Behaviour of α- and β-CaSO4 · 0,5 H2O as a Function of Crystal Structure and Morphology. *Cryst. Res. Technol.* **2002**, *37* (10), 1075−1087.
(29) Crowley, J. K. Visible and near-infrared (0.4−2.5 μm) reflectance spectra of Playa evaporite minerals. *J. Geophys. Res.* **1991**, *96* (B10), 16231.
(30) Blaney, D. L.; McCord, T. B. Indications of sulfate minerals in the Martian soil from Earth-based spectroscopy. *J. Geophys. Res.* **1995**, *100* (E7), 14433.
(31) Prasad, P. S. R.; Chaitanya, V. K.; Prasad, K. S.; Rao, D. N. Direct formation of the γ-CaSO4 phase in dehydration process of gypsum: In situ FTIR study. *Am. Mineral.* **2005**, *90* (4), 672−678.
(32) Prieto-Taboada, N.; Larrañaga, a.; Gómez-Laserna, O.; Martínez-Arkarazo, I.; Olazabal, M. a.; Madariaga, J. M. The relevance of the combination of XRD and Raman spectroscopy for the characterization of the $CaSO_4$-H_2O system compounds. *Microchem. J.* **2015**, *122*, 102−109.
(33) Carreño-Márquez, I. J. A.; Castillo-Sandoval, I.; Esparza-Ponce, H. E.; Fuentes-Cobas, L. E.; Montero-Cabrera, M. E. Characterization of gypsum crystals exposed to a high CO_2 concentration fog using X-Ray. In *RADIATION PHYSICS: XI International Symposium on Radiation Physics*, Ciudad Juárez, Chih., Mexico, March 4−6, 2015; AIP Publishing LLC, 2015; Vol. *1671*, p 030006.
(34) Menéndez, E.; Matschei, T.; Glasser, F. P. Sulfate Attack on Concrete. In *Performance of Cement-Based Materials in Aggressive Aqueous Environments*; Springer: Dordrecht, Netherlands, 2013; pp 7−74.
(35) Torrance, A.; Darvell, B. W. Effect of humidity on calcium sulphate hemihydrate. *Aust. Dent. J.* **1990**, *35* (3), 230−235.
(36) Mannsfeld, S. C. X-ray scattering from polycrystalline monolayers and thin films. In *6th Annual SSRL School on Synchrotron X-ray Scattering Techniques in Materials and Environmental Sciences: Theory and Application*, Menlo Park, CA, May 29−31, 2012; U.S. Department of Energy: Washington, DC, 2012.
(37) Burciaga-Valencia, D. C.; Villalobos-Portillo, E. E.; Marín-Romero, J. A.; Sánchez del Río, M.; Montero-Cabrera, M. E.; Fuentes-Cobas, L. E.; Fuentes-Montero, L. Recent developments in the texture analysis program ANAELU. *J. Mater. Sci.: Mater. Electron.* **2018**, 1−7.
(38) *ICDD PDF-4+*; Kabekkodu, S., Ed.; International Centre for Diffraction Data: Newtown Square, PA, 2014.
(39) Auvray, C.; Homand, F.; Sorgi, C. The aging of gypsum in underground mines. *Eng. Geol.* **2004**, *74* (3−4), 183−196.
(40) Garofalo, P. S.; Fricker, M. B.; Günther, D.; Forti, P.; Mercuri, A.-M.; Loreti, M.; Capaccioni, B. Climatic control on the growth of gigantic gypsum crystals within hypogenic caves (Naica mine, Mexico). *Earth Planet. Sci. Lett.* **2010**, *289* (3−4), 560−569.
(41) Sipple, E.-M.; Bracconi, P.; Dufour, P.; Mutin, J.-C. Microstructural modifications resulting from the dehydration of gypsum. *Solid State Ionics* **2001**, *141−142*, 447−454.

DOI: 10.1021/acs.cgd.8b00583
Cryst. Growth Des. 2018, 18, 4611−4620

(42) Fowler, A.; Howell, H. G.; Schiller, K. K. The dihydrate-hemihydrate transformation in gypsum. *J. Appl. Chem.* **1968**, *18* (12), 366−372.
(43) Chen, Z.; Sucech, S.; Faber, K. T. A hierarchical study of the mechanical properties of gypsum. *J. Mater. Sci.* **2010**, *45* (16), 4444−4453.
(44) Murrell, S. A. F.; Ismail, I. A. H. The effect of decomposition of hydrous minerals on the mechanical properties of rocks at high pressures and temperatures. *Tectonophysics* **1976**, *31* (3−4), 207−258.
(45) Fan, C.; Teng, H. H. Surface behavior of gypsum during dissolution. *Chem. Geol.* **2007**, *245* (3−4), 242−253.
(46) Finot, E.; Lesniewska, E.; Mutin, J. C.; Goudonnet, J. P. Reactivity of gypsum faces according to the relative humidity by scanning force microscopy. *Surf. Sci.* **1997**, *384* (1−3), 201−217.
(47) Fernández-Cortes, A.; Calaforra, J. M.; Sánchez-Martos, F.). Spatiotemporal analysis of air conditions as a tool for the environmental management of a show cave (Cueva del Agua, Spain). *Atmos. Environ.* **2006**, *40* (38), 7378−7394.
(48) Sarma, L. P.; Prasad, P. S. R.; Ravikumar, N. Raman spectroscopic study of phase transitions in natural gypsum. *J. Raman Spectrosc.* **1998**, *29* (9), 851−856.
(49) Lane, M. D. Mid-infrared emission spectroscopy of sulfate and sulfate-bearing minerals. *Am. Mineral.* **2007**, *92* (1), 1−18.
(50) He, B. B. *Two-Dimensional X-ray Diffraction*; Wiley: New York, 2011; pp 56−63.
(51) Jacques, S. D. M.; González-Saborido, A.; Leynaud, O.; Bensted, J.; Tyrer, M.; Greaves, R. I. W.; Barnes, P. Structural evolution during the dehydration of gypsum materials. *Mineral. Mag.* **2009**, *73* (3), 421−432.
(52) Chang, R. *Chemistry*, 7th ed.; McGraw Hill: New York, p 1088.
(53) Wray, J. J.; Squyres, S. W.; Roach, L. H.; Bishop, J. L.; Mustard, J. F.; Noe Dobrea, E. Z. Identification of the Ca-sulfate bassanite in Mawrth Vallis, Mars. *Icarus* **2010**, *209* (2), 416−421.
(54) Ossorio, M.; Van Driessche, a. E. S.; Pérez, P.; García-Ruiz, J. M. The gypsum−anhydrite paradox revisited. *Chem. Geol.* **2014**, *386*, 16−21.
(55) Van Driessche, A. E. S.; Benning, L. G.; Rodriguez-Blanco, J. D.; Ossorio, M.; Bots, P.; García-Ruiz, J. M. The Role and Implications of Bassanite as a Stable Precursor Phase to Gypsum Precipitation. *Science* **2012**, *336* (6077), 69−72.
(56) Ruiz-Agudo, E.; Álvarez-Lloret, P.; Ibañez-Velasco, A.; Ortega-Huertas, M. Crystallographic Control in the Replacement of Calcite by Calcium Sulfates. *Cryst. Growth Des.* **2016**, *16* (9), 4950−4959.
(57) Wondyfraw, M. Mechanisms and Effects of Acid Rain on Environment. *J. Earth Sci. Clim. Change* **2014**, *5* (6), 204.

DOI: 10.1021/acs.cgd.8b00583
Cryst. Growth Des. 2018, 18, 4611−4620